Desalination and Water Treatment
www.deswater.com

22 (2010) 161–173
October

1944-3994/1944-3986
doi: 10/5004/dwt.2010.1393

Development of an integrated reverse osmosis-greenhouse system driven by solar photovoltaic generators

P.A. Davies*, A.K. Hossain

Sustainable Environment Research Group, School of Engineering and Applied Science, Aston University, Birmingham B4 7ET, UK
Tel. +44 121 204 3724; email: p.a.davies@aston.ac.uk

Received 30 November 2009; Accepted 26 April 2010

ABSTRACT

The development of a system that integrates reverse osmosis (RO) with a horticultural greenhouse has been advanced through laboratory experiments. In this concept, intended for the inland desalination of brackish groundwater in dry areas, the RO concentrate will be reduced in volume by passing it through the evaporative cooling pads of the greenhouse. The system will be powered by solar photovoltaics (PV). Using a solar array simulator, we have verified that the RO can operate with varying power input and recovery rates to meet the water demands for irrigation and cooling of a greenhouse in north-west India. Cooling requires ventilation by a fan which has also been built, tested and optimised with a PV module outdoors. Results from the experiments with these two subsystems (RO and fan) are compared to theoretical predictions to reach conclusions about energy usage, sizing and cost. For example, the optimal sizing for the RO system is 0.12–1.3 m^2 of PV module per m^2 of membrane, depending on feed salinity. For the fan, the PV module area equals that of the fan aperture. The fan consumes <30 J of electrical energy per m^3 of air moved which is 3 times less than that of standard fans. The specific energy consumption of the RO, at 1–2.3 kWh m^{-3}, is comparable to that reported by others. Now that the subsystems have been verified, the next step will be to integrate and test the whole system in the field.

Keywords: Reverse osmosis; Concentrate disposal; Solar PV; Greenhouse; Brackish water

1. Introduction

This study is motivated by the need for technology to treat and manage saline groundwater so that it can be used sustainably in agriculture. The use of saline groundwater for irrigation is one factor contributing to the salinity and sodicity of soils which are problems reported to affect some 8% of the world's land surface. Australia is the country having the largest salt-affected area; other countries significantly affected include Egypt and India [1].

The excess or imbalance of salts can impair soil structure and inhibit the uptake of water and nutrients by crops. Consequently crops yields are typically decreased [2]. This is particularly problematic for developing countries such as India, where a burgeoning population places growing demands on food supplies and water resources, increasing the pressure to use waters of marginal quality, such as urban wastewater and saline and sodic groundwater.

Salinisation is widespread in the north-western states of India, which have been chosen as the geographical focus of this study. Thus the states of Gujarat, Rajasthan and Haryana have 2.23, 0.38 and 0.23 million hectares of salt-affected land, respectively. In the state of Rajasthan, it is reported that 'more than 80% of the groundwater resources are of poor quality and are unfit for irrigation of agricultural crops' [1]. The rainfall of north-west India is seasonal and ranges from below 300 mm/year in West Rajasthan to

*Corresponding author.

approaching 700 mm/year closer to Delhi, while temperatures frequently exceed 40°C in the dry season and solar irradiation is about 2,000 kWh/m^2 per year [3]. Such arid or semi-arid conditions greatly restrict agriculture through rain-fed irrigation. Therefore there is a pressing need for new approaches to groundwater treatment and water conservation in this region.

Reverse osmosis (RO) using membranes can help address the salinity problem, as this technology removes sodium chloride and other salts from water. The modest energy usage of RO compared to other (e.g. thermal) desalination technologies makes it an attractive option. The low osmotic pressure of brackish water means that the energy requirements for RO are especially low for this type of feed. However, besides giving purified water, RO also rejects a stream of concentrated brine which can aggravate the salinisation and degradation of land if this concentrate is not disposed of carefully. Currently, the main approach to the management of the rejected concentrate is through reduction of its volume and precipitation to solid, using for example evaporation ponds or spray dryers [4]. Solid salts are more easily contained than a larger volume of brine and in some cases it may be possible to sell them for use in chemical or food industries.

In a previous concept study, a novel method to reduce the volume of concentrate was put forward whereby it is used for evaporative cooling of a greenhouse [5]. In this concept, the concentrate is no longer regarded as a waste stream; instead it provides a useful substitute for the water that would otherwise be required for the cooling process. The evaporation pond, though still needed for final reduction to solid, will be smaller than would otherwise be the case.

Another benefit of this concept, which is illustrated in Fig. 1, is that water is conserved inside the greenhouse due to the low evapotranspiration compared to outside. Irrigation can be provided by the permeate water from the RO. Thus both the permeate and concentrate outputs from the RO are fed to the greenhouse. To favour use in remote locations and reduce reliance on conventional energy sources, it is proposed to drive the fans and pumps of the system using solar energy captured by photovoltaic (PV) panels. The earlier study analysed theoretically the mass and energy balance, optimum sizing and costs of the whole system [5].

The aim here is to develop this system to a point where it can be practically implemented. The main objective is to verify the key subsystems, namely the PV-powered

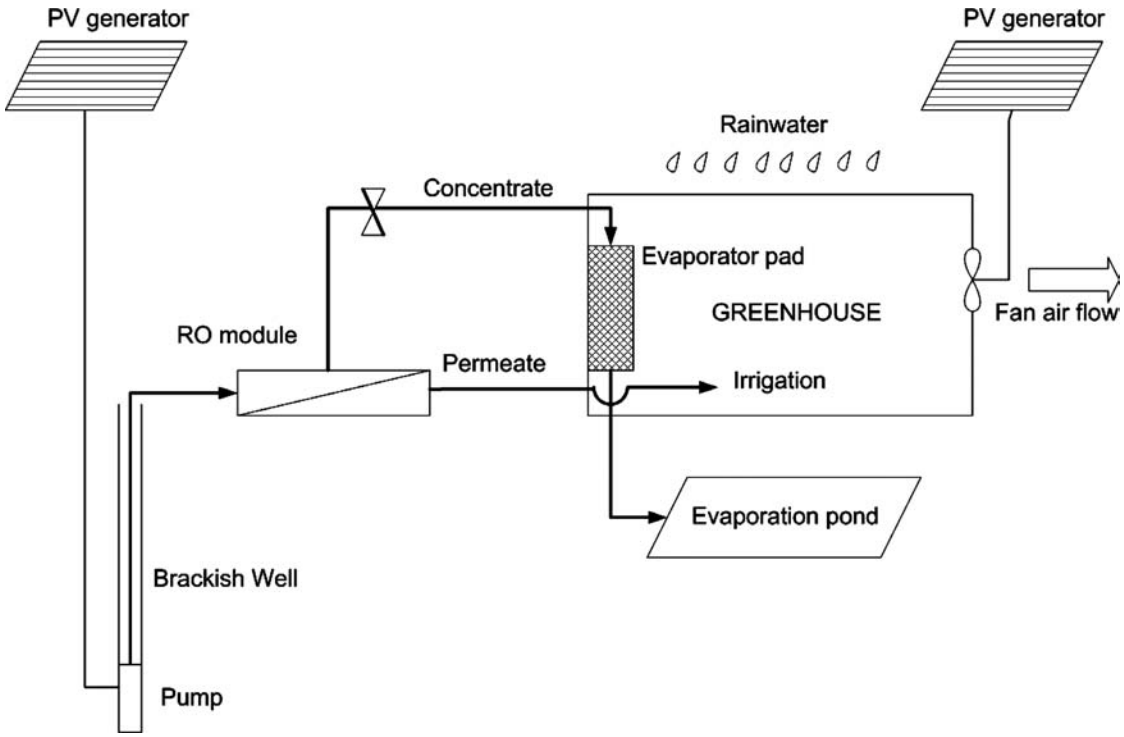

Fig. 1. Schematic of the overall concept integrating RO, an evaporatively-cooled greenhouse and PV generators (reproduced from [5]).

RO and the PV-powered fan which have been built and tested in the laboratory. (Note that the evaporative cooler has already been reported on elsewhere [6]). We will report on the experience gained with each of these and compare the results against the theoretical predictions. A further objective is to provide simple formulae and guidelines for the sizing of the main components.

General goals in the design of these subsystems are: (i) simplicity, to be achieved through the use of few components which should be durable and ideally off-the-shelf; (ii) minimisation of energy usage to reduce the cost of the PV generator; and (iii) effective electrical matching of the PV generator and loads to maintain performance under varying operating conditions. The detailed development of each of these two subsystems, RO and fan, will now be described separately.

2. PV-powered RO subsystem

RO systems have evolved through the use of conventional power sources but in recent years the use of renewable energy has become of increasing interest. Among renewable energy sources, solar in particular has great potential given that the need for desalination typically coincides with high solar radiation. In a recent review, Ghermandi and Massalen [7] have identified some 79 solar-RO systems that have been built or designed worldwide. Those actually built are of small capacity (less than 100 m^3 daily output) and are currently cost competitive only in locations remote from grid power. To cite a recent example, Banat et al. have installed and evaluated in Jordan a PV-RO desalinator for brackish water giving an output of about 0.4 m^3 per day [8].

On the other hand, much larger systems (up to 2,000 m^3/day output, or greater for hybrid systems) are on the drawing board. In the future, solar-RO could supply a significant amount of desalinated water but the main barrier to this happening is, according to Ghermandi and Massalen, an economic one. Therefore it is very important to look into ways of minimising cost.

There are several approaches to building a PV-RO system. One that has been quite common is to connect PV panels to a battery bank which then drives standard AC motors and pumps via a frequency inverter. This has the advantage of enabling very standard equipment to be used. However, as pointed out by several authors [9–12], systems without batteries are potentially more reliable and cost-effective. It is generally less expensive and more efficient to store the product water in tanks than the corresponding electrical energy in batteries. A possible risk, however, in using battery-less systems is that they must accommodate the power fluctuations that occur as the sunlight varies diurnally and seasonally [12]. At low power input, the flux of water across the membrane decreases causing permeate salinity to increase. The design must take this condition into account to maintain an output of sufficient quality.

For inland desalination, the concentrate from an RO system represents wastage in terms of both energy and water. Here there is a fundamental conflict in the sense that, as more permeate is recovered, the osmotic pressure and theoretical energy requirement increases. To maximise recovery without excessive energy consumption, Singh has proposed ingenious arrangements involving multiple pumps and membrane stages [13]. In the current project, an alternative approach is pursued in which the concentrate is used to provide another function, namely evaporative cooling, thus simplifying the design in situations where such cooling is needed.

2.1. Theory

The theory used to describe the RO process uses the following well known equations to represent the transport of water and salt across the membrane of area A_{mem} (m^2) [14]:

$$\frac{Q_{perm}}{A_{mem}} = S\left(\Delta p - \Delta p_{osm}\right) \tag{1}$$

and

$$\frac{\dot{m}_{salt}}{A_{mem}} = B\Delta c \tag{2}$$

The relations used to calculate the osmotic pressure Δp_{osm}(Pa) and the concentration difference are as reported previously [5]. The Eq. (1) predicts a linear relation of the permeate flux Q_{perm}/A_{mem} (ms^{-1}) to the net driving pressure $\Delta p - \Delta p_{osm}$ and Eq. (2) predicts a linear relation of the salt mass flux $\dot{m}_{perm}/A_{mem}$ ($kgm^{-2}s^{-1}$) to the concentration difference Δc (kgm^3) across the membrane. Thus experiments can be carried out to test this linearity and to determine the membrane permeability S ($ms^{-1}Pa^{-1}$) and the salt transport coefficient B (ms^{-1}). Earlier, values of S and B were calculated from the manufacturer's data sheets and, to facilitate comparisons with the experimental results, they are repeated here in Table 1 [15].

A key insight from the earlier study was a simple method for estimating the optimum economic size of the PV-powered pump ($\hat{P}_{PVpump}$, measured in peak electrical watts) relative to the RO membrane area A_{mem} [5].Thus:

$$\frac{\hat{P}_{PVpump}}{A_{mem}} = \frac{Q_{perm}}{A_{mem} r \eta \kappa}\left(\Delta p_{osm} + \rho g d + \frac{Q_{perm}}{A_{mem} S}\right) \tag{3}$$

Table 1
Properties of membranes tested in this study, based on the manufacturer's data [15]

Type	Manufacturer's code	Permeability (S)/10^{-11} ms^{-1}Pa^{-1}	Salt transport coefficient (B) /10^{-7} m s^{-1}	At feed salinity (c_{feed})/ppm
Low energy	XLE-2540	2.2	1.2	500
Brackish water	BW30-2540	1.0	0.59	2000

where the optimum flux is the greater of the following two:

$$\frac{Q_{perm}}{A_{mem}} = \sqrt{r\kappa\eta S \frac{C_{mem}}{C_{PVpump}}} \tag{4}$$

or

$$\frac{Q_{perm}}{A_{mem}} = B\alpha \frac{c_{feed}}{c_{permeate}} \tag{5}$$

In these equations, d (m) is the depth of the well in which the pump is inserted, g (ms^{-2}) is acceleration due to gravity, r is the recovery rate, α is the ratio of the spatial average of the concentration at the membrane surface to the feed concentration, ρ is the density of water, η is the pump efficiency and κ is a capacity factor evaluated over the operational day (i.e. the energy captured by the PV as fraction of that captured if exposed to full sunlight at 1,000 Wm^{-2} for the part of the day when it operates). The terms C_{mem} and C_{PVpump} are the costs of the membrane (€ m^{-2}) and of the PV-pump (€ per peak watt) respectively; c_{feed} and $c_{permeate}$ (ppm) are the concentrations of salt in the respective streams.

If the size of the system is already known and it is desired to predict output, the following expression (derived as the solution of the quadratic Eq. (3)) is useful:

$$Q_{perm} = \frac{-\Delta p_{osm} AS + \sqrt{\left(\Delta p_{osm} AS\right)^2 - 4r\eta\kappa AS\hat{P}_{PVpump}}}{2} \tag{6}$$

Whereas strictly Eqs. (3)–(6) describe the instantaneous behaviour of the time-varying system, here they are used to represent average quantities over the operational day.

2.2. Experimental equipment

To avoid the need for batteries, a positive displacement pump was preferred due to its ability to maintain high efficiency over a range of power input levels and output pressures corresponding to varying sunlight and flow. In contrast, a centrifugal pump tends to require constant power input, making it less suitable. A progressive cavity pump (also called a helical rotor or Moineau pump) was selected since, in addition to having the advantage of being a positive displacement device, it can by virtue of its compact design serve both to extract water from a borehole and to pressurise it for feeding to the RO membranes. The need for a second pump is therefore avoided. Note, however, that the pump specified previously was not available [5]; therefore a slightly less efficient model had to be substituted.

A rig was constructed in the laboratory as shown by the schematic in Fig. 2 by using the bill of materials shown in Table 2. Since this type of system is modular, such that performance is essentially independent of size, the rig was made as small as permitted by the size of the available pump. Accordingly, the permeate output was nominally 1 m^3 per day. Three 2.5″ diameter RO modules were connected in parallel to give a total membrane area of 7.8 m^2. The relative sizing between the PV-pumping system was guided by the economic considerations analysed earlier [5], which led to input power levels in the range 150–300 W peak. This power

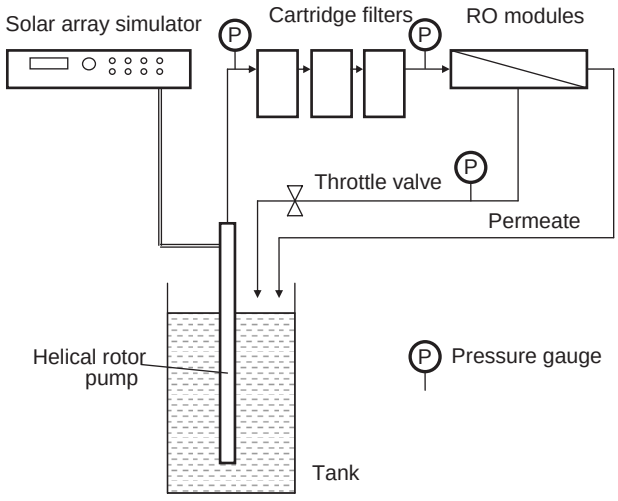

Fig. 2. Schematic of the RO rig tested in the laboratory with the objective of verifying the concept of Fig. 1. Note that the RO stage, depicted for simplicity as a single unit, actually consisted of 3 identical modules connected in parallel.

Table 2
Bill of materials for the RO rig shown in Fig. 2

Description	Quantity	Make/model	Details/specification
Solar array simulator	1	Agilent E4360	Maximum output 510 W, V_α = 65 V, I_α = 8.5 A. Factory calibrated.
Helical Rotor Pump	1	Grundfos SQF 0.6–2	3″ diameter stainless steel borehole pump with integrated controller and maximum power-point tracking
Tank	1	_	500 litre capacity, polypropylene
Cartridge filter no.1	1	Parker M19R10A-RS	10 micron polypropylene wound depth filter
Cartridge filter no.2	1	Pentek NCP-10	10 micron carbon impregnated polyester pleated filter
Cartridge filter no.3	1	Parker M39R10A-RS	1 micron polypropylene wound depth filter
RO module	3	Dow Corning XLE-2540 or BW30-2540	See Table 1
Pressure vessel	3	_	GRP type, 2.5″ diameter × 40″ long
Pressure gauge	3	_	100 mm diameter liquid-filled analogue type, 0–16 bar, calibrated. Accuracy ± 0.1 bar.
Throttle valve	1	George Fischer	1/2″ diaphragm type

was provided by a solar simulator whose current-voltage characteristics were set to replicate the output from commercially available PV modules situated in the Delhi climate, as the target location for this project is north-west India. As indicated in Tables 1 and 2, two membrane types were tested: the low energy type (XLE) and the brackish water type (BW30).

2.3. Experimental method

To test how faithfully Eqs. (1) and (2) represent the real system, and to simulate operation in the field, experiments were carried out at different salinities, power inputs, driving pressures and recovery rates. Saline solutions were made up by adding sodium chloride (general purpose grade) to tap water (of conductivity <0.2 dSm^{-1}) to give solutions of concentrations <100, 500, 1,000, 2,000, 5,000 and 10,000 ppm. This is representative of the range of groundwater salinities typically encountered in Haryana and Rajasthan. To neutralise chlorine in the tap water and inhibit bacterial growth, sodium metabisulphite was added at a concentration of 2 ppm.

In each of the first series of experiments, inlet pressure was stepped in increments of 1 bar by gradual closing of the throttle valve until recovery reached 70%, while the input power to the pump was held constant at the values shown in Table 3. After each change in pressure, an interval of 15 mins was allowed for the conditions to stabilise. Flow rates at the two outlets were then measured by weighing samples collected over one minute. The salinity of these samples was determined using a conductivity probe (Hanna HI 8733). Pressures were measured at the inlet and outlet of the RO modules using calibrated gauges.

The second series of experiments was designed to simulate whole-day operation. In each of these, the input power to the pump was varied to simulate typical sunlight in Delhi over the course of one day, based on a PV array size of 300 W peak, while the throttle valve remained at a constant setting. Typical solar days for the months of April (representing the dry season), August (representing summer) and December (representing winter) were constructed from published meteorological data [16]. The setting of the throttle valve was in each case chosen so as to provide the differing recovery rates needed for the greenhouse according to seasonal variations in sunlight and humidity [2]. Whereas the data represented hourly changes, the rig conditions were changed half-hourly; in other words the experiment was carried out at an accelerated rate of twice the real speed. The feed salinity was 2,000 ppm for the XLE membrane and 5,000 ppm for the BW30 membrane.

Both series of experiments were repeated for each of the two membranes tested. The temperature of the water in the tank, which varied from 20.5 to 23.5 °C, was measured using a mercury-in-glass thermometer (accuracy ± 0.25 °C) at the beginning and end of every experiment so that a temperature correction factor could be applied to normalise the permeate flux to 25 °C using tables in reference [17].

2.4. Results and analysis

The results from the pressure-stepping experiments are shown in Fig. 3, which plots the temperature-corrected permeate flux against net driving pressure, and in Fig. 4 which plots the mass flux of salt across the

Table 3
Power input settings used for the pressure-stepping experiments with the RO system, also showing the results for permeability S from the pressure-stepping experiments, obtained by straight line to fit to Figs. 3 and 4 (values of regression coefficient R^2 are shown in brackets)

Membrane type	Feedwater salinity (c_{feed})/ppm	Pump input power/W	Permeability (S)/10^{-11} ms^{-1}Pa^{-1}
XLE	<100	150	1.88 (0.917)
	500	150	1.62 (0.945)
	1,000	150	1.64 (0.942)
	2,000	200	1.45 (0.938)
	5,000	300	1.01 (0.963)
BW30	<100	300	0.95 (0.997)
	1,000	300	0.86 (0.996)
	2,000	300	0.85 (0.989)
	5,000	300	0.80 (0.980)
	10,000	300	0.73 (0.988)

membrane against concentration difference. It can be seen from Fig. 3 that the permeability S of both membranes decreases with increasing salt concentration in the feed. The permeability of the XLE membrane decreases not only with concentration but with pressure also; this may be due to compaction of the membrane. The values of S obtained by least-squares fit for each of the membranes and feed concentrations are presented in Table 3. Compared to the values expected from Table 1, the measured value for the BW30 membrane is 15% lower; this may be explained by manufacturing tolerances and experimental error. For the XLE membrane, the measured permeability is 26% lower; this suggests partial fouling in spite of the pre-treatment filters used.

The measured value of salt transport coefficient, B, however, is independent of feed concentration and pressure for both membranes tested. This is seen from Fig. 4 which shows consistent linearity over a range of feed concentrations. Straight line fits give $B = 2.9 \times 10^{-7}$ and 1.8×10^{-7} ms^{-1} for the XLE and BW membrane respectively. This exceeds by a factor of 2.4 and 3 respectively the values in Table 1, reflecting a much larger than expected passage of salt through the membrane. Consequently, the XLE membrane is not suitable for feed salinities above about 2,000 ppm in the solar-powered application, as the permeate salinity will increase above 500 ppm. The BW30 may be used instead as it has higher salt rejection, but with a penalty of increased energy requirement due to the lower permeability of this membrane.

A sample of the results from the whole-day simulation of experiments is shown in Fig. 5. Table 4

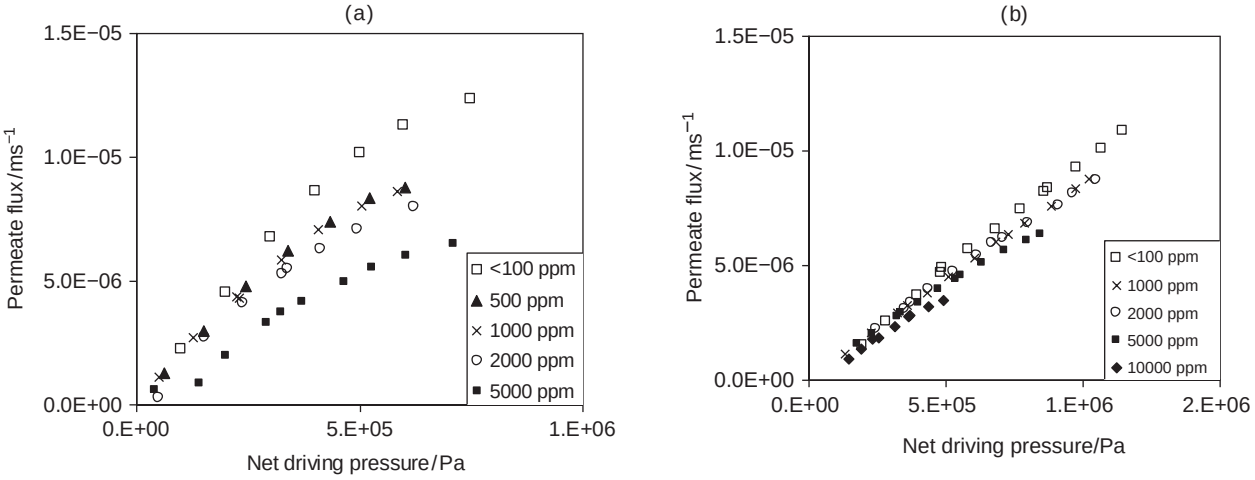

Fig. 3. Results obtained with the RO rig, as used for the determination of permeability S, showing permeate flux versus net driving pressure for: (a) the XLE membrane; and (b) the BW30 membrane.

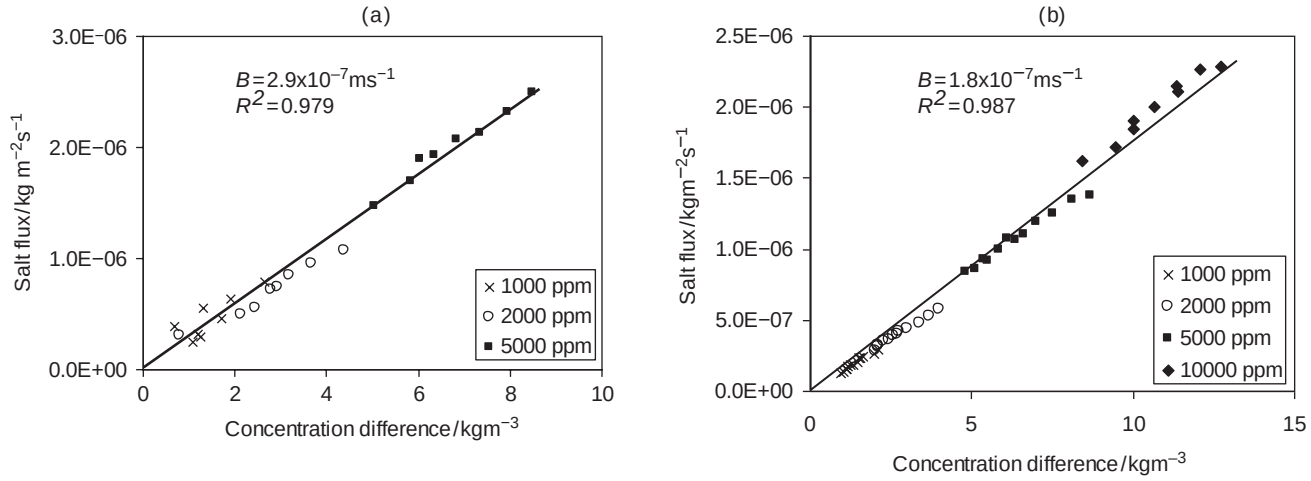

Fig. 4. Results obtained with the RO rig, as used for the determination of salt transport coefficient *B*, showing mass flux of salt versus the concentration difference across the membrane for: (a) the XLE membrane; and (b) the BW30 membrane.

summarises the performance for each of the three months tested. As the average solar irradiation for the three months considered (April, August and December) is very close to that for the whole year in Delhi, whole year performance is readily obtained from these results and is also included in Table 4. The specific energy consumption is in the range 1–2.3 kWh/m^3 which is comparable to results reported in the literature [7].

It is interesting to compare the measured permeate output (nominally 1 m^3/day) with that predicted by Eq. (6). Fig. 6 shows that, for the XLE membrane, the measured output is up to 36% less than predicted on the basis of the membrane properties and pump efficiencies derived from the manufacturers' data. When the properties observed in the pressure-stepping experiments of this study are used instead, the agreement is to within a few percent. For the BW30 membrane, the discrepancy with prediction is smaller (<21%) because the observed properties were closer to those derived from the manufacturers' data in this case.

Based on these experimental findings, revised relative sizes and system parameters are shown in Table 5. As a result of lower membrane permeability, higher salt transport coefficient and lower pump efficiency, the overall cost is increased by some 30–80 over that calculated previously. Note that, to enable a consistent comparison, the same component costs and currency exchange rates have been used as in reference [5].

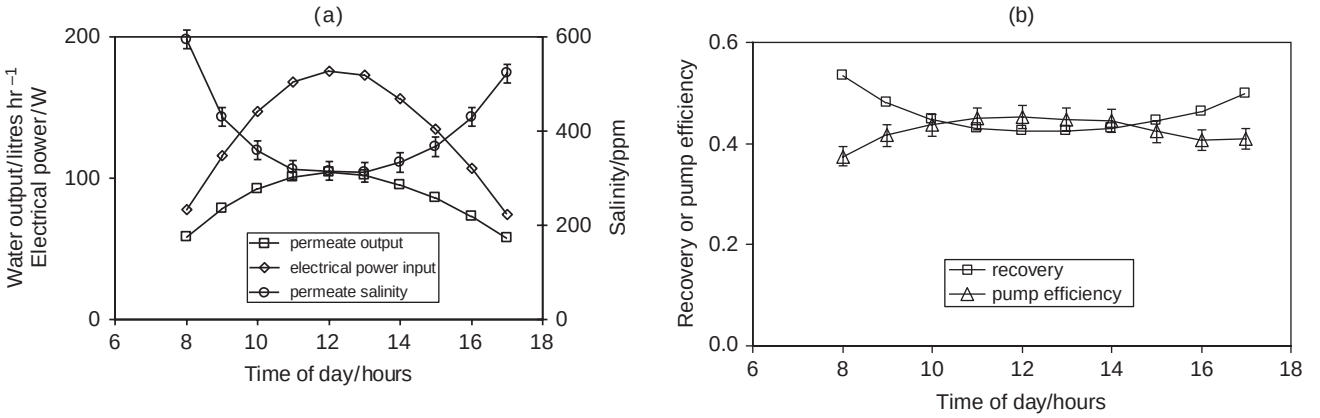

Fig. 5. Sample results from whole-day simulation experiments with the RO rig showing: (a) permeate output, electrical power input for pump and salinity of permeate; and (b) pump efficiency and recovery. Feed salinity 5,000 ppm, membrane type BW30, month of August (monsoon season).

Table 4
Summarised results from whole-day simulation experiments, for two different membranes and three months of the year each representing a different season. Calculated results for the whole year are also shown

Membrane	Feed salinity (c_{feed})/ ppm	Month	Totals over 1 d			Averages over 1 d			
			Permeate output/m^3	Concentrate output/m^3	Electrical input/ kWh	Permeate salinity/ ppm	Recovery	Pump efficiency	Specific energy usage/kWh m^{-3}
XLE	1,000	April	1.024	3.135	1.72	128	0.25	0.30	1.68
		August	1.259	1.811	1.33	145	0.41	0.37	1.06
		December	0.962	1.851	1.15	158	0.34	0.32	1.19
		Whole year	1.082	2.265	1.40	144	0.32	0.33	1.29
BW30	5,000	April	0.777	2.184	1.72	334	0.26	0.43	2.22
		August	0.848	1.038	1.33	381	0.45	0.43	1.57
		December	0.599	1.253	1.07	411	0.32	0.44	1.79
		Whole year	0.741	1.492	1.37	375	0.33	0.43	1.85

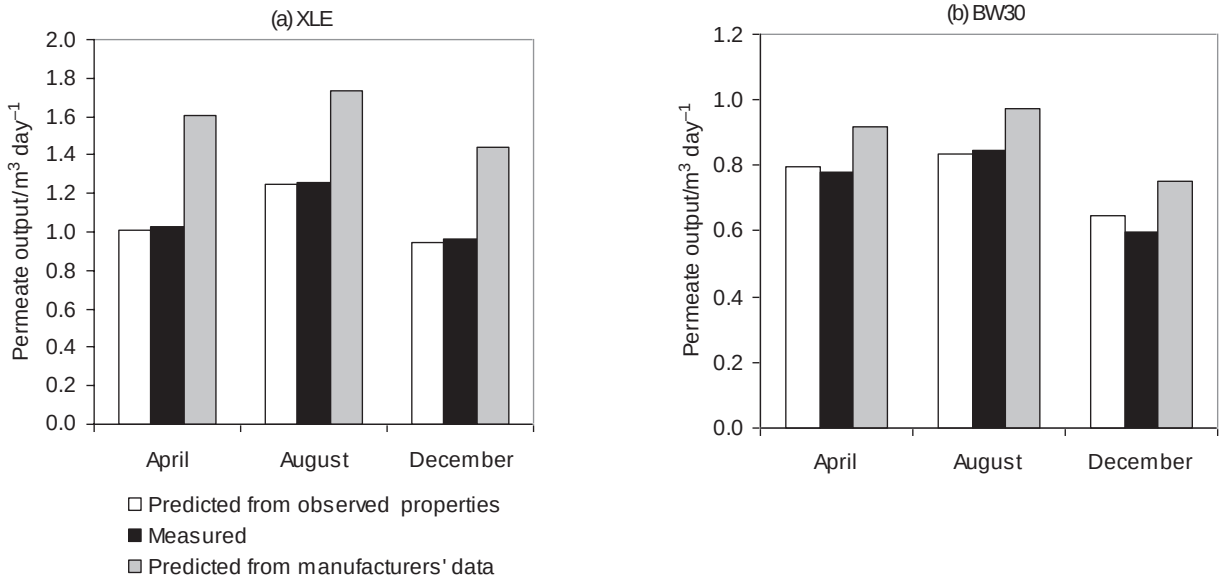

Fig. 6. Comparison of measured quantities of permeate output (as in Table 4) with those predicted from Eq. (6), based on observed properties and on manufacturers' data (a) XLE membrane; and (b) BW30 membrane.

3. PV-powered fan subsystem

The purpose of the fan is to evaporate water from the concentrate, thereby reducing its volume, at the same time providing a cooling effect favourable to plant growth in the greenhouse. Though the theory of PV-powered fans was discussed some 30 years ago [18], only recently have versions intended for greenhouse cooling become commercially available, and still there is a lack of larger fans of this type.

It is possible to use a conventional fan, having an AC induction motor, and couple this to PV by means of a frequency inverter. However, the energy consumption of available fans exceeds 90 J per m^3 of air moved. This would result in a high system cost due to the large PV generator needed. As shown by an earlier study [19], considerable energy may be saved through operation at reduced speed. It was also shown that, below a certain speed, the energy savings with standard AC induction motors are limited and that greater saving can be achieved using a DC motor. The latter approach is therefore adopted here.

3.1. Theory

For the optimisation of the PV-powered fan operation, it is useful to have a mathematical model to

Table 5
Optimum sizing of the PV generator to the RO system for minimum cost, based on the values of *S* and *B* determined from the experiments

Well depth *(d)*/m	Feed salinity (c_{feed})/ppm	Membrane	Membrane area (A_{mem})/ m²	Typical pump outlet pressure/ bar	Typical permeate flux/10^{-6} ms^{-1}	Economic sizing PV/RO		System cost for 1 m³ daily output of permeate/€
						Peak electrical power per membrane area/Wm^{-2}	Area PV module/ area of RO membrane	
0	2,000	XLE	11.1	4.2	2.5	16	0.12	3040
0	5,000	BW30	9.5	9.9	2.9	44	0.32	5800
0	10,000	BW30	4.8	20.4	5.8	183	1.3	10800
10	5,000	BW30	9.5	10.9	2.9	49	0.35	6320

$r = 0.35$, $\eta = 0.4$, $C_{mem} = 80$ €m^{-2}, $C_{PVpump} = 12$ € W^{-1}. Areas of PV module are based on a solar to electrical conversion efficiency of 14%.

represent the performance of both the fan and the PV generator. The current-voltage relation for a DC motor coupled to a fan via a belt with reduction ratio x is given by Eq. (7) [19]:

$$I_m = (k_1 k_v^2 / \chi^3 k_T) V_m^2 \quad (7)$$

where k_1 (Ws³) is a constant which, multiplied by the cube of the rotational speed, gives the power consumption of the fan; k_T (NmA^{-1}) is the torque constant of the motor, k_v (s^{-1}V^{-1}) is the speed constant of the motor; I_m (A) is the current in the motor and V_m (*V*) is the voltage across it. The following equation relates the current I_{PV} and the voltage V_{PV} generated by a PV generator, on the basis of an the equivalent circuit consisting of a current source, a diode and a series resistor R_S(Ω) [20].

$$V_{PV} = V_{oc} - I_{PV} R_s + nmV_t \ln(1 - I_{PV}/I_L) \quad (8)$$

where V_{oc} is the open-circuit voltage, n is the number of cells connected in series within the module, V_t is the thermal voltage (nominally 0.025 V at 300 K) and m is a number between 1 and 2. The value of the photo-generated current I_L is taken to be equal to the short-circuit current, and is proportional to the solar irradiance G (Wm^{-2}). The value of V_{oc} at a given level of irradiance G is given by:

$$V_{oc} = V_{oc0} + nmV_t \ln(G/G_0) \quad (9)$$

where G_0 is the nominal level of irradiance for which V_{oc0} is already known. The values of the constants m and R_s appearing in Eqs. (8) and (9) were adjusted to match the characteristics stated by the manufacturer of the solar module at nominal operating conditions corresponding to solar irradiance of 800 Wm^{-2}. Thus the current-voltage curves for different light levels have been plotted in Fig. 7.

3.2. Experimental equipment

To ensure longevity of the DC motor, a brushless type with electronic commutation was selected as motor brushes inevitably need replacing within a few months of use. A practical issue to be addressed in coupling to the fan was that of obtaining a sufficient reduction

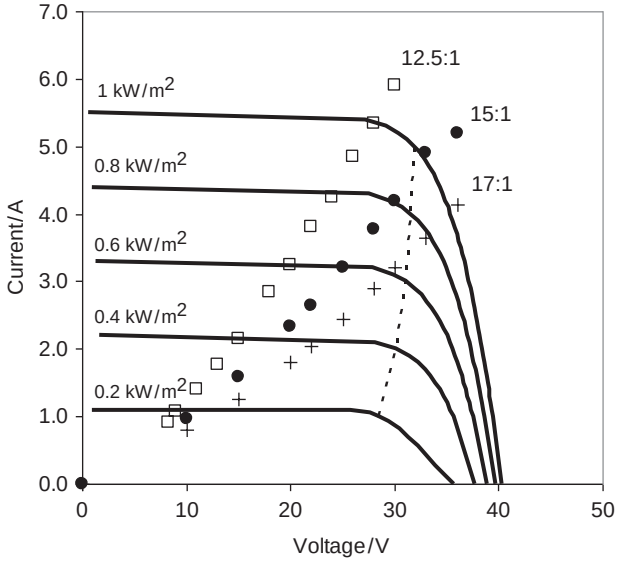

Fig. 7. Current-voltage characteristics for the PV generator and for the DC motor-fan. Solid lines represent the PV generator at different irradiance levels, on the basis of Eqs. (4) and (5), while the broken line shows the locus of the maximum power point of the generator. Markers show the measurements for the motor-fan at three different gearing ratios.

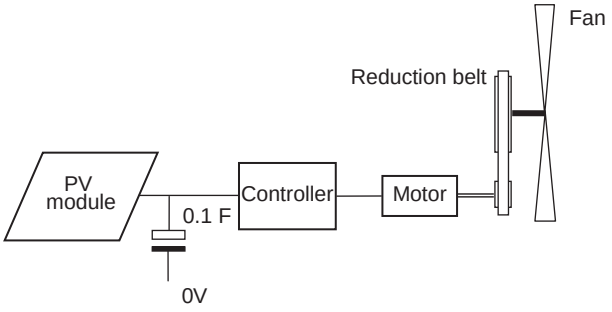

Fig. 8. Experimental set up for the solar-powered fan tested with the objective of verifying the concept of Fig. 1.

gearing ratio for optimal matching. Preliminary calculations based on the above theory indicated that a ratio of about 1:15 ($x = 1/15$) would be needed for operation at the maximum power point of the PV module. To minimise mechanical losses, it was desirable to achieve this in a single stage. This means that the driving pulley must be small (about 20 mm diameter) to suit the existing large pulley of the fan hub. Therefore the drive belt was selected carefully to give adequate flexibility to wrap around the small pulley while maintaining sufficient strength and endurance.

Preliminary experiments showed difficulty starting at low light levels. The high starting torque and current caused the voltage to dip and the controller to cut out. Sometimes the system entered a state of repeated starting and stalling. This was overcome by connecting a capacitor in parallel with the supply from the PV module.

Based on the above considerations, the experimental apparatus shown in Fig. 8 was constructed. Table 6 lists the main parts used.

3.3. Experimental procedure

Two series of experiments were conducted. In the first, intended to optimise the gearing ratio, the PV generator of Fig. 8 was replaced by a bench top power supply which was used to measure the current-voltage characteristic of the fan-motor with different sizes of the driving pulley, giving gear ratios of 12.5:1, 15:1 and 17:1. The voltage was increased in increments of 5 V upto 40 V. At each setting, current was measured and the rotation speed was measured using a stroboscope.

In the second series of experiments, the fan was connected to a PV module which was located outdoors in Birmingham, UK. The PV module was in a shadow free position and facing south with an inclination of 25° to the horizontal. Measurements were taken of the electrical conditions of the fan, rotation speed and solar irradiance (using a pyranometer, Kipp and Zonen CM3). As a test of endurance, the system was left to run continually and without operator intervention for a period of 83 days during the summer of 2009, with measurements repeated every few days.

3.4. Results and analysis

Fig. 7 superimposes, for different gearing ratios, the current-voltage characteristics of the motor on those of the PV generator. To select the optimum gearing ratio, it is desirable that the curves intersect at the maximum power point of the generator. A perfect match is only achievable for a single level of irradiance, however. Therefore the gearing ratio should ideally be altered according to the light level. Nonetheless, the effect of changing the gear ratio is in practice modest, as shown by Fig. 9 where the airflow has been plotted against irradiance for different gearing ratios based on intersections of the curves in Fig. 7. A larger reduction ratio (i.e. more revolutions of the motor per revolution of the fan blades) favours high air flow at low light levels, whereas a smaller ratio increases air flow at high light levels at the expense of flow at the low levels.

Table 6
Bill of materials for the solar-powered fan set up shown in

Description	Quantity	Make/model	Details/specifications
Fan	1	Multifan–130	50″ diameter, 3 blades
PV module	1	BP 4175	175 W peak output, Va = 43.6 V_α and I_{sc} = 5.45 A at standard test conditions. Dimensions 1.6 × 0.8 m
Capacitor	1	–	Electrolytic, 0.1 F, 40 V
Controller	1	Maxon DEC 50/5	1 quadrant amplifier Rated 5 A continuous (10 A peak), 1–50 VDC
Motor	1	Delta Precision Motors 57BL116	Brushless DC Rated 4,000 rpm at 36 V, k_T = 15.9 $AN^{-1}m^{-1}$
Reduction belt	1	Contitech	Timing belt 10 mm wide × 5 mm pitch
Pulley	1	Contitech	Timing belt pulley 10 mm wide × 5 mm pitch, 12 teeth*

*Various pulley sizes were used to achieve different gearing ratios.

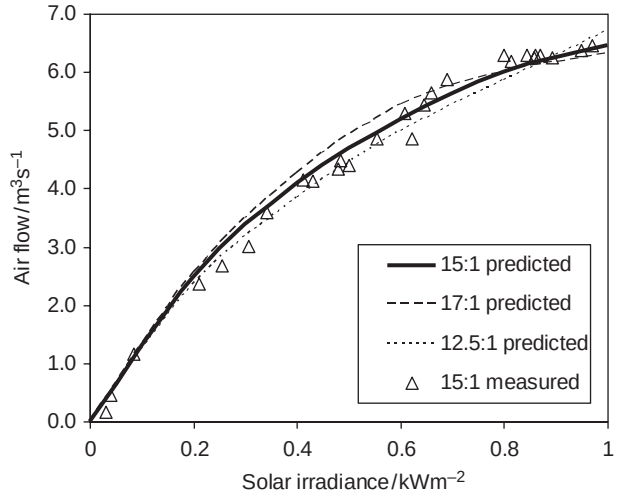

Fig. 9. Air flow vs. solar irradiance for the solar-powered fan for three different gearing ratios, based on predictions from Fig. 7, and measured with a PV module outdoors.

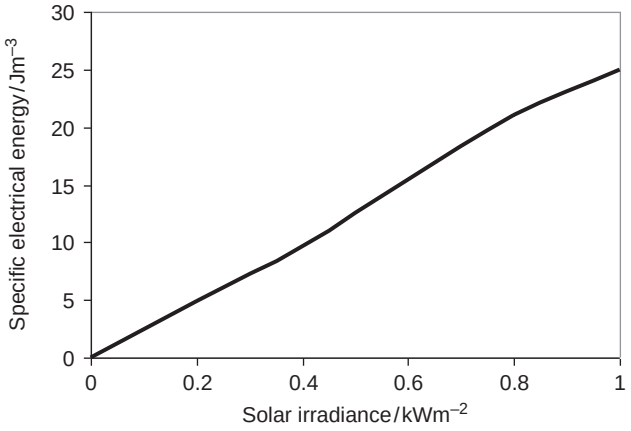

Fig. 10. Specific electrical energy expressed as joules per cubic metre of air moved, based on Fig. 8 (gearing 15:1).

Note that the airflow shown in Fig. 9 is that at <10 Pa static pressure. As is the case with all the air flow data given here, it is based on the measured rotation speed converted to airflow by means of a table provided by the fan manufacturer for the fan fitted with an expansion cone. Fig. 9 also shows, on the same basis, results from the second series of experiments in which the fan was run from the PV module. Fig. 10 shows the specific energy consumption of the solar-powered fan as a function of solar irradiance; it is seen to be below 30 J per m^3 of air moved.

The results from the endurance test are shown in Fig. 11 which shows that after 83 days of running, including automatic start-up and shut-down, there was no deterioration in the performance of the system.

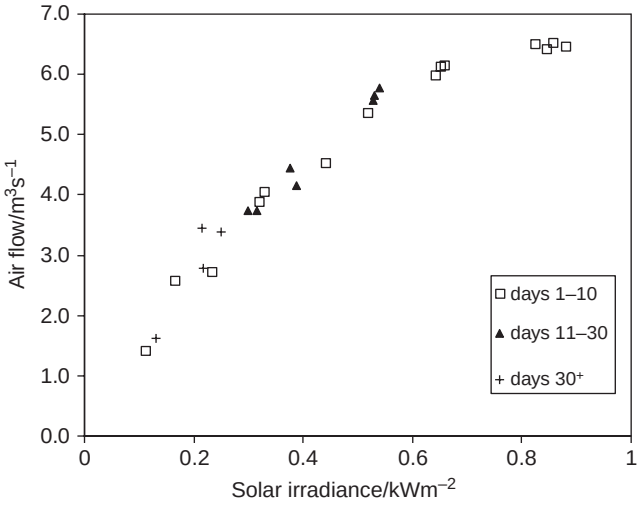

Fig. 11. Results from endurance test conducted over 83 days with the motor-fan powered from the PV module outdoors.

4. Conclusions

Motivated by the opportunity to develop an integrated RO-greenhouse system that desalinates brackish groundwater with minimal discharge of liquid concentrate, this work has investigated experimentally the use of PV-powered subsystems, namely the RO unit and a ventilation fan. In the experiments with the RO, two membrane types have been tested with salinities up to 10,000 ppm NaCl. The theory used to choose the optimal sizing of the PV generator has been verified; however, it was found important to use observed rather than stated values of component properties, otherwise the theory tends to overestimate water output and underestimate salt flux.

Based on these experiments, the estimates of the capital cost of the main components (i.e. PV-pump and RO membranes) of the PV-RO desalination subsystem have increased above those reported in the earlier theoretical study [5]. For example, for a PV-RO subsystem taking feed water of salinity 5,000 ppm from a well 10 m deep and producing 1 m^3 per day of permeate, the cost has increased by 58% from 4,000 to 6,320 €. Nevertheless, this results in only an 11% increase in the cost of the whole system including the greenhouse and fans.

The performance of the solar-powered fan has matched theoretical expectations. As a result of slower rotation speed and the use of a more efficient motor, the specific energy consumption is below 30 J per m^3 of air moved, which is three times less than that of commercially available fans. The speed of the fan responds automatically to levels of sunlight and is therefore synchronised to cooling requirements. After 83 days of operation the fan has shown very good reliability.

Further testing will be carried out to establish reliability over longer periods.

From these experiments and the supporting theory, simple guidelines have been deduced for the appropriate sizing of the PV generators. Thus, for the RO subsystem, 0.12 m^2 of PV panel is needed per m^2 of membrane with feed water at 2,000 ppm salinity, increasing to 1.3 m^2 per m^2 at 10,000 ppm salinity. For the fan, the PV module should have an area equivalent to the fan aperture, where the peak air speed should be about 5 ms^{-1}. Though based on the climate of Delhi, where solar irradiation averages about 5 kWh m^{-2} day^{-1}, these guidelines are expected to remain approximately valid for other similarly sunny locations where the technology may be deployed. Countries besides India where solar desalination of brackish groundwater is needed and already being evaluated include Australia, Egypt, Jordan, Mexico, Oman, Saudi Arabia, Tunisia and the USA [7].

Together with the preceding studies [5,6,19], this work has confirmed the technical feasibility of the integrated PV-RO-Greenhouse concept, based on experiments in the laboratory using made up salt solutions. The next step will be to construct and test the whole system in India with a brackish groundwater source.

Acknowledgement

Financial support from the Engineering and Physical Sciences Research Council of the UK is acknowledged (grant reference EP/E044360/1). The authors also thank Vostermans BV for providing fan performance data.

Symbols

A_{mem} — area of membrane, m^2
B — salt transport coefficient, ms^{-1}
c_{feed} — salt concentration in feed, ppm
$c_{permeate}$ — salt concentration in permeate, ppm
C_{mem} — cost of RO membrane per area, € m^{-2}
C_{PVpump} — cost of PV-pump system per peak watt, € W^{-1}
d — well depth, m
g — acceleration due to gravity, ms^{-2}
G — solar irradiance, Wm^{-2}
I_L — photo-generated current, A
I_m — current in motor windings, A
I_{PV} — current from PV generator, A
k_1 — constant in fan law, Ws^3
k_T — motor torque constant, NmA^{-1}
k_v — motor voltage constant, $s^{-1}V^{-1}$
M — constant characterising PV generator
n — number of PV cells in series
$\dot{m}_{salt}$ — mass flow rate of salt, kgs^{-1}
Δp — transmembrane pressure, Pa
Δp_{osm} — osmotic pressure across membrane, Pa
$\hat{P}_{PVpump}$ — peak electrical power of PV-pump, W
Q_{perm} — discharge of permeate, m^3s^{-1}
r — recovery rate
R — regression coefficient
R_s — series resistance, Ω
S — permeability of membrane to water, $ms^{-1}Pa^{-1}$
V_m — voltage across motor windings, V
V_{PV} — voltage from PV generator, V
V_α — open circuit voltage of PV generator, V
V_t — thermal voltage of PV generator, V
α — ratio of the wall concentration to c_{feed}
χ — belt reduction ratio
η — efficiency of PV-pump system
κ — capacity factor during operational time
ρ — density of water, kg m^{-3}

References

[1] G. Singh, Salinity-related desertificatioin and management strategies: Indian experience. Land Degradation and Development, 20(2009) 367–385.
[2] M. Qadir, Agricultural use of marginal-quality water: opportunities and challenges, in Water for food, water for life: A Comprehensive Assessment of Water Mangement in Agriculture, D. Molden (Ed.) 2007, Earthscan: London.
[3] India Meteorological Department website. [cited 2010; Available from: http://www.imd.gov.in].
[4] L.F. Greenlee, Reverse osmosis desalination: Water sources, technology, and today's challenges. Water Res., 43 (9) (2009) 2317–2348.
[5] P.A. Davies, D.K. Hossain and P. Vasudevan, Stand-alone groundwater esalination system using reverse osmosis combined with a cooled greenhouse for use in arid and semi-arid zones of India. Desalin. and Water Treat., 5 (2009) 223–234.
[6] A.K. Hossain and P.A. Davies, Small-scale reverse osmosis brackish water desalting system combined with greenhouse application for use in remote arid communities. Desalin. and Water Treat., 3 (2009) 229–235.
[7] A. Ghermandi and R. Messalem, Solar-driven desalination with reverse osmosis: The state of the art. Desalin. and Water Treat., 7 (2009) 285–296.
[8] F. Banat, H. Qiblawey and Q. Al-Nasser, Economic evaluation of a small RO unit powered by PV installed in the village of Hartha, Jordan. Desalin. and Water Treat., 3 (2009) 169–174.
[9] M. Thomson and D. Infield, A photovoltaic-powered seawater reverse-osmosis system without batteries. Desalin, 153 (1–3) (2003) 1–8.
[10] M. Thomson and D. Infield, Laboratory demonstration of a photovoltaic-powered seawater reverse-osmosis system without batteries. Desalin, 183 (1–3) (2005) 105–111.
[11] A.I. Schäffer, A. Broeckmann and B.S. Richards, Renewable Energy Powered Membrane Technology 1. Development and characterization of a photovoltaic hybrid membrane system. Environ. Sci. Technol., 41 (2007) 998–1003.
[12] B.S. Richards, D.P.S. Capão and A.I. Schäffer, Renewable Energy Powered Membrane Technology. 2. The Effect of Energy Fluctuations on Performance of a Photovoltaic Hybrid Membrane System. Environ. Sci. Technol., 42 (2008) 4563–4569.

[13] R. Singh, Brine recovery at industrial RO plants: Conceptual process design studies. Desalin. and Water Treat., 8 (2009) 54–67.
[14] M. Wilf, The Guidebook to Membrane Desalination Technol., 2007: Balaban.
[15] FILMTEC Membranes Product Information Form 609-00350-0408 and Form 609-00349-0706, Dow Chemical Company.
[16] ISHRAE, India Weather Data Set. 2005: Indian Society of Heating Refrigerating and Air-Conditioning Engineers.
[17] FILMTEC Reverse Osmosis Membranes Technical Manual. 2005, Dow Chemical Company.
[18] J.A. Roger, Theory of the direct coupling between d. c. motors and photovoltaic solar arrays. Solar Energy, 23(3) (1979) 193–198.
[19] P.A. Davies et al. Energy saving and solar electricity in fan-ventilated greenhouses. Acta Hortic., 797 (2008) 95–101.
[20] E. Lorenzo, Solar Electricity, 1994: Progensa.